

Redox Behavior of Rhodium 9,10-Phenanthrenediimine Complexes

David W. Shaffer, Scott A. Ryken, Ryan A. Zarkesh, and Alan F. Heyduk*

Department of Chemistry, University of California, Irvine (UCI), California 92697-2025

Received April 20, 2010

New square-planar rhodium complexes of the redox-active ligand 9,10-phenanthrenediimine (phdi) have been prepared and studied. The complexes [dpp-nacnac^{CH₃}]Rh(phdi) (**2a**; [dpp-nacnac^{CH₃}][−] = CH[C(Me)(N-Pr₂C₆H₃)₂][−]) and [dpp-nacnac^{CF₃}]Rh(phdi) (**2b**; [dpp-nacnac^{CF₃}][−] = CH[C(CF₃)(N-Pr₂C₆H₃)₂][−]) have been prepared from the corresponding [nacnac]Rh(CO)₂ synthons by treatment with Me₃NO in the presence of the phdi ligand. Complexes **2a** and **2b** are diamagnetic, and their absorption spectra are dominated by intense charge-transfer transitions throughout the visible region. Electrochemical studies indicate that both the phdi ligand and the rhodium metal center are redox-active, with the [nacnac][−] ligands serving to modulate the one-electron-oxidation and -reduction redox potentials. In the case of **2a**, chemical oxidation and reduction reactions provided access to the one-electron-oxidized cation, [2a]⁺, and one-electron-reduced anion, [2a][−], the latter of which has been characterized in the solid state by single-crystal X-ray diffraction. Solution electron paramagnetic resonance spectra of [2a]⁺ and [2a][−] are consistent with S = 1/2 spin systems, but surprisingly the low-temperature spectrum of [2a][−] shows a high degree of rhombicity, suggestive of rhodium(II) character in the reduced anion.

Introduction

Late-transition-metal ions interact with redox-active ligands to afford complexes with complicated electronic properties owing to the energetic proximity of the metal d orbitals and the frontier ligand orbitals.¹ Ambiguity in the assignment of metal and ligand oxidation states often arises in these types of complexes, prompting them to be described as noninnocent.² Protocols have been established for utilizing structural, spectroscopic, and theoretical techniques to probe the electronic structures of these complexes,^{1e,3} and as such, there has

been an increase in the study of the synthesis and reactivity of these complexes.^{1,3,4} Surprisingly, despite the importance of rhodium complexes to coordination, bioinorganic, and organometallic chemistry, little effort has been directed toward understanding the electronic properties of rhodium complexes with such redox-active ligands.^{1d,5,6}

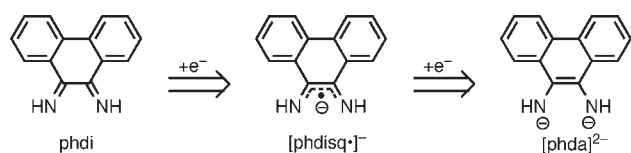
Square-planar rhodium(I) complexes occupy a special position in inorganic and organometallic chemistry for their dynamic stoichiometric and catalytic bond activation reactivity.⁷ In addition to the catalysis of a variety of H–X additions to unsaturated organic substrates,⁸ rhodium(I) complexes have been exploited in hydrogen production from protons,⁹ CO₂ reduction,¹⁰ and C–F activation¹¹ and have even been shown to bind N₂.¹² One of the key features of square-planar rhodium(I) complexes that leads to this varied

*To whom correspondence should be addressed. E-mail: aheyduk@uci.edu.

- (1) (a) Ghosh, M.; Weyhermüller, T.; Wieghardt, K. *Dalton Trans.* **2010**, 39, 1996–2007. (b) Chirik, P. J.; Wieghardt, K. *Science* **2010**, 327, 794–795. (c) Boyer, J. L.; Rochford, J.; Tsai, M.-K.; Muckerman, J. T.; Fujita, E. *Coord. Chem. Rev.* **2010**, 254, 309–330. (d) van der Vlugt, J. I.; Reek, J. N. H. *Angew. Chem., Int. Ed.* **2009**, 48, 8832–8846. (e) Kaim, W.; Lahiri, G. K. *Angew. Chem., Int. Ed.* **2007**, 46, 1778–1796. (f) de Bruin, B.; Hettterscheid, D. G. H. *Eur. J. Inorg. Chem.* **2007**, 211–230. (g) Butin, K. P.; Beloglazkina, E. K.; Zyk, N. V. *Russ. Chem. Rev.* **2005**, 74, 531–553. (h) Ward, M. D.; McCleverty, J. A. *J. Chem. Soc., Dalton Trans.* **2002**, 275–288.
- (2) (a) Kaim, W.; Schwederski, B. *Pure Appl. Chem.* **2004**, 76, 351–364. (b) Jørgensen, C. K. *Coord. Chem. Rev.* **1966**, 1, 164–178. (c) Jørgensen, C. K. *Oxidation Numbers and Oxidation States*; Springer: Heidelberg, Germany, 1969.
- (3) (a) Ray, K.; Petrenko, T.; Wieghardt, K.; Neese, F. *Dalton Trans.* **2007**, 1552–1566. (b) Remenyi, C.; Kaupp, M. *J. Am. Chem. Soc.* **2005**, 127, 11399–11413. (c) Lever, A. B. P.; Gorelsky, S. I. *Struct. Bonding (Berlin)* **2004**, 107, 77–114. (d) Chaudhuri, P.; Verani, C. N.; Bill, E.; Bothe, E.; Weyhermüller, T.; Wieghardt, K. *J. Am. Chem. Soc.* **2001**, 123, 2213–2223.
- (4) (a) Lippert, C. A.; Arnstein, S. A.; Sherrill, C. D.; Soper, J. D. *J. Am. Chem. Soc.* **2010**, 132, 3879–3892. (b) Kaim, W.; Sieger, M.; Greulich, S.; Sarkar, B.; Fiedler, J.; Zálaiš, S. *J. Organomet. Chem.* **2010**, 695, 1052–1058. (c) Roquette, P.; Maronna, A.; Peters, A.; Kaifer, E.; Himmel, H.-J.; Hauf, C.; Herz, V.; Schiedt, E.-W.; Scherer, W. *Chem.—Eur. J.* **2010**, 16, 1336–1350. (d) McKinnon, S. D. J.; Patrick, B. O.; Lever, A. B. P.; Hicks, R. G. *Chem. Commun.* **2010**, 46, 773–775.

- (5) Allgeier, A. M.; Mirkin, C. A. *Angew. Chem., Int. Ed.* **1998**, 37, 895–908.
- (6) Palmer, J. H.; Mahammed, A.; Lancaster, K. M.; Gross, Z.; Gray, H. B. *Inorg. Chem.* **2009**, 48, 9308–9315.
- (7) Colby, D. A.; Bergman, R. G.; Ellman, J. A. *Chem. Rev.* **2010**, 110, 624–655.
- (8) (a) Lazzaroni, R.; Settambolo, R.; Alagone, G.; Ghio, C. *Coord. Chem. Rev.* **2010**, 254, 696–706. (b) Hayashi, T.; Yamasaki, K. *Chem. Rev.* **2003**, 103, 2829–2844. (c) *Rhodium-Catalysed Hydroformylation*; van Leeuwen, P. W. N. M., Claver, C., Eds.; Kluwer CMC: Dordrecht, The Netherlands, 2000. (d) Ritleng, V.; Sirlin, C.; Pfeffer, M. *Chem. Rev.* **2002**, 102, 1731–1769.
- (9) Grass, V.; Lexa, D.; Savéant, J.-M. *J. Am. Chem. Soc.* **1997**, 119, 7526–7532.
- (10) Huang, K.-W.; Han, J. H.; Musgrave, C. B.; Fujita, E. *Organometallics* **2007**, 26, 508–513.
- (11) Torrens, H. *Coord. Chem. Rev.* **2005**, 249, 1957–1985.
- (12) (a) Masuda, J. D.; Stephan, D. W. *Can. J. Chem.* **2005**, 83, 324–327. (b) Budzelaar, P. H. M.; de Gelder, R.; Gal, A. W. *Organometallics* **1998**, 17, 4121–4123. (c) Vignalok, A.; Ben-David, Y.; Milstein, D. *Organometallics* **1996**, 15, 1839–1844.

Chart 1



reactivity is the nucleophilicity of the metal center, which provides a mechanism for the binding of substrates in the metal coordination sphere.

The introduction of a redox-active ligand into the coordination sphere of a rhodium(I) center offers a unique opportunity to compliment the nucleophilicity of rhodium(I) with a ligand capable of further two-electron reactivity. 9,10-Phenanthrene-diimine (phdi) is a redox-active ligand derived from phenanthrenequinone in which the quinone oxygen atoms have been replaced with imines to afford an α -diimine for coordination to metal ions. While phdi has been utilized extensively as a ligand for rhodium(III) and other metal ions for DNA intercalation studies,¹³ its use as a platform for redox activity with lower-valent late transition metals is underexplored.^{14,15} While phdi is a closed-shell neutral ligand, one-electron reduction affords an open-shell diiminosemiquinonate ([phdisq]^{•-}) and two-electron reduction affords the closed-shell phenanthrenediimide form ([phda]²⁻), as shown in Chart 1. Thus, a Rh^Iphdi complex could be bifunctional in that the rhodium(I) metal center would be nucleophilic because of its d⁸ electron configuration and yet the complex could still be reduced by up to two electrons because of the redox-active nature of the phdi ligand. This paper reports the synthesis of a new type of rhodium(I) complex that includes a redox-active phdi ligand and a chelating [nacnac]⁻ ligand. While the neutral complex displays properties consistent with a “normal” square-planar, d⁸ rhodium(I) coordinated to a phdi ligand, one-electron oxidation and reduction afford complexes that display noninnocent behavior. Notably, the electron paramagnetic resonance (EPR) spectra for the one-electron-reduction product suggest oxidation of the metal center up to rhodium(II) with concomitant reduction of the phdi ligand to the [phda]²⁻ oxidation state.

Experimental Section

General Considerations. Many of the complexes described below are air- and moisture-sensitive, necessitating that manipulations be carried out under an inert atmosphere of argon or nitrogen using standard Schlenk, vacuum-line, and glovebox techniques. All reactions were carried out at ambient temperature (20–24 °C) unless otherwise noted. Hydrocarbon solvents were sparged with argon, then deoxygenated, and dried by successive passage through Q5 and activated alumina columns, respectively. Etheral and halogenated solvents were sparged with argon and then dried by passage through two activated alumina columns. To test for effective oxygen and water removal, nonchlorinated solvents were treated with a few drops of a purple solution of sodium benzophenone ketyl in tetrahydrofuran (THF). The ligand precursors *N,N'*-bis-

(trimethylsilyl)-9,10-phenanthrenediimine,¹⁶ [dpp-nacnac^{CF3}]⁻H,¹⁷ and [dpp-nacnac^{CH3}]⁻Li·Et₃O¹⁸ were prepared according to established procedures. Graphite (Alfa Aesar) was dried under a dynamic vacuum at <0.1 mtorr for 1 day prior to use. Potassium metal (Alfa Aesar) and [RhCl(CO)₂]₂ (Heraeus) were used without further purification.

Physical Methods. NMR spectra were collected on Bruker Avance 400 and 600 MHz spectrometers in dry, degassed CDCl₃ or C₆D₆. ¹H NMR spectra were referenced to tetramethylsilane (TMS) using the residual proteo impurities of the solvent; ¹³C NMR spectra were referenced to TMS using the natural abundance ¹³C impurities of the solvent. ¹⁹F NMR spectra were referenced to CFCl₃ using C₆F₆ as an internal standard at -164.9 ppm. All chemical shifts are reported using the standard δ notation in parts per million; positive chemical shifts are to a higher frequency from the given reference. IR spectra were recorded as KBr pellets with a Perkin-Elmer Spectrum One FTIR spectrophotometer. Electronic absorption spectra were recorded with a Perkin-Elmer Lambda 800 UV-vis spectrophotometer. APCI-MS data were collected on a Waters LCT Premier mass spectrometer. Perpendicular-mode X-band EPR spectra were collected using a Bruker EMX spectrometer equipped with an ER041XG microwave bridge.

Electrochemical Methods. Electrochemical experiments were performed on a Gamry Series G 300 potentiostat/galvanostat/ZRA (Gamry Instruments, Warminster, PA) using a 3.0 mm glassy carbon working electrode, a platinum wire auxiliary electrode, and a silver wire reference electrode. Electrochemical experiments were performed at ambient temperature (20–24 °C), either in a nitrogen-filled glovebox or under an atmosphere of argon. Sample concentrations were 1.0 mM in THF with 0.10 M NBu₄PF₆ as the supporting electrolyte. All potentials are referenced to [Cp₂Fe]^{+0,19} using decamethylferrocene as an internal standard (-0.49 V vs [Cp₂Fe]⁺⁰). The typical solvent system window with our configuration was +1.0 V for the oxidation limit and -3.4 V for the reduction limit (vs [Cp₂Fe]⁺⁰). Decamethylferrocene (Acros) was purified by sublimation under reduced pressure,²⁰ and tetrabutylammonium hexafluorophosphate (Acros) was recrystallized from ethanol three times and dried under vacuum.²¹

Synthesis of 9,10-Phenanthrenediimine (phdi) and 9,10-Phenanthrenediimine-*d*₂ (phdi-*d*₂). The synthesis was through modification of a published procedure.¹⁶ Dry methanol (50 mL) was added to a Schlenk flask containing 487 mg of *N,N'*-bis-(trimethylsilyl)-9,10-phenanthrenediimine (1.39 mmol) and stirred for 40 min. The solvent and methoxytrimethylsilane byproduct were then removed under reduced pressure. Pure phdi was isolated in quantitative yield as a light-green solid. The deuterated version, phdi-*d*₂, was prepared by an analogous procedure using methanol-*d*. Anal. Calcd for C₁₄H₁₀N₂: C, 81.53; H, 4.89; N, 13.58. Found: C, 81.06; H, 4.69; N, 13.37. ESI-MS (methanol): *m/z* 207.0 ([M + H]⁺). ¹H NMR (C₆D₆, 600 MHz): δ 12.39 [s, 1H, N-H, (*E,Z*)-phdi], 10.47 [s, 1H, N-H, (*E,Z*)-phdi], 10.18 [s, 2H, N-H, (*Z,Z*)-phdi], 8.89 [d, ³J_{HH} = 7 Hz, 1H, Ar-H, (*E,Z*)-phdi], 8.60 [d, ³J_{HH} = 7 Hz, 2H, Ar-H, (*Z,Z*)-phdi], 7.48 (m, Ar-H), 7.10 (t, Ar-H), 7.07 (t, Ar-H), 7.00 (t, Ar-H), 6.85 (d, Ar-H), 6.78 (t, Ar-H). IR (KBr): ν_{CO} 3252 (N-H), 3208 (N-H), 3065 (N-H), 1624 (C=N), 1602 (C=N) cm⁻¹. UV-vis [CH₂Cl₂; λ_{max}/nm ($\epsilon/M^{-1} cm^{-1}$): 296 (3200), 373 (1900).

(13) (a) Fu, P. K.-L.; Bradley, P. M.; Turro, C. *Inorg. Chem.* **2003**, *42*, 878–884. (b) Hall, D. B.; Holmlin, R. E.; Barton, J. K. *Nature* **1996**, *382*, 731–735. (c) Krotz, A. H.; Kuo, L. Y.; Barton, J. K. *Inorg. Chem.* **1993**, *32*, 5963–5974.

(14) Belsler, P.; Von Zelewsky, A.; Zehnder, M. *Inorg. Chem.* **1981**, *20*, 3098–3103.

(15) (a) Chern, S.-S.; Liaw, M.-C.; Peng, S.-M. *J. Chem. Soc., Chem. Commun.* **1993**, 359–361. (b) Peng, S. M.; Chen, C.-T.; Liaw, D.-S.; Chen, C.-I.; Wang, Y. *Inorg. Chim. Acta* **1985**, *101*, L31–L33.

(16) Tuchtenhagen, G.; Rühlmann, K. *Liebigs Ann. Chem.* **1968**, *711*, 174–183.

(17) van Belzan, R.; Klein, R. A.; Smeets, W. J. J.; Spek, A. L.; Benedix, R.; Elsevier, C. *J. Recl. Trav. Chim. Pays-Bas* **1996**, *115*, 275–285.

(18) Stender, M.; Wright, R. J.; Eichler, B. E.; Prust, J.; Olmstead, M. M.; Roesky, H. W.; Power, P. P. *J. Chem. Soc., Dalton Trans.* **2001**, 3465–3469.

(19) (a) Connelly, N. G.; Geiger, W. E. *Chem. Rev.* **1996**, *92*, 877–910. (b) Gritzner, G.; Kuta, J. *Pure Appl. Chem.* **1984**, *56*, 461–466.

(20) (a) Zahl, A.; van Eldik, R.; Matsumoto, M.; Swaddle, T. W. *Inorg. Chem.* **2003**, *42*, 3718–3722. (b) Coddington, J.; Wherland, S. *Inorg. Chim. Acta* **1996**, *242*, 159–164.

(21) Bedard, R. L.; Dahl, L. F. *J. Am. Chem. Soc.* **1986**, *108*, 5933–5942.

Synthesis of [dpp-nacnac^{CF3}]⁺Li·Et₂O. A solution of [dpp-nacnac^{CF3}]⁺H (151 mg, 287 mmol, 1 equiv) in 9 mL of pentane and 1 mL of diethyl ether was cooled to $-35\text{ }^{\circ}\text{C}$. *n*-BuLi (2.60 M, 121 μL , 1.1 equiv) in hexane was diluted to 5 mL in pentane and added dropwise to the [dpp-nacnac^{CF3}]⁺H solution. After stirring at room temperature for 12 h, the solvent was reduced to 2 mL, when the product began to precipitate. The suspension was warmed to redissolve all solids and then cooled to $-35\text{ }^{\circ}\text{C}$ to precipitate the product as yellow crystals (yield 119 mg, 69%). ¹H NMR (CDCl₃, 600 MHz): δ 7.06 (d, ³J_{HH} = 7.3 Hz, 4H, Ar-*H*), 7.06 (t, ³J_{HH} = 7.6 Hz, 2H, Ar-*H*), 5.52 (s, 1H, -*CH*-), 2.97 [sept, ³J_{HH} = 6.9 Hz, 4H, -CH(CH₃)(CH₃)'], 2.69 (br, 4H, -OCH₂CH₃), 1.22 [d, ³J_{HH} = 6.8 Hz, 12H, -CH(CH₃)(CH₃)'], 1.03 [d, ³J_{HH} = 6.9 Hz, 12H, -CH(CH₃)(CH₃)'], 0.67 (br, 6H, -OCH₂CH₃). ¹³C NMR (CDCl₃, 125.8 MHz): δ 152.5 (q, ²J_{CF} = 68 Hz, CN), 145.9 (aryl-CN), 139.9 (*o*-aryl-C), 124.3 (aryl-C), 123.5 (aryl-C), 83.4 (-CH-), 28.3 [-CH(CH₃)(CH₃)'], 25.0 [-CH(CH₃)(CH₃)'], 23.1 [-CH(CH₃)(CH₃)']. ¹⁹F NMR (CDCl₃, 376.5 MHz): δ -64.0 (s, 6F, -CF₃).

Synthesis of [dpp-nacnac^{CH3}]⁺Rh(CO)₂ (1a). A 5 mL ether solution containing 387 mg of [dpp-nacnac^{CH3}]⁺Li·Et₂O (776 μmol , 2.0 equiv) was added to 151 mg of [Rh(μ -Cl)(CO)₂]₂ (389 μmol , 1 equiv) dissolved in 5 mL of ether. The yellow solution was stirred for 8 h. After filtration to remove LiCl, the solvent was removed under reduced pressure. Yellow crystals (yield 347 mg, 78%) of the product were obtained after recrystallization of the crude product from THF at $-35\text{ }^{\circ}\text{C}$. Anal. Calcd for C₃₁H₄₁N₂O₂Rh: C, 64.58; H, 7.17; N, 4.86. Found: C, 64.45; H, 7.25; N, 4.80. ¹H NMR (CDCl₃, 500 MHz): δ 7.20–7.13 (m, 6H, Ar-*H*), 5.12 (s, 1H, -*CH*-), 3.23 [sept, ³J_{HH} = 6.9 Hz, 4H, -CH(CH₃)(CH₃)'], 1.79 (s, 6H, -CH₃), 1.37 [d, ³J_{HH} = 6.8 Hz, 12H, -CH(CH₃)(CH₃)'], 1.22 [d, ³J_{HH} = 7.0 Hz, 12H, -CH(CH₃)(CH₃)']. ¹³C NMR (CDCl₃, 125.8 MHz): δ 184.2 (d, ¹J_{RhC} = 66 Hz, CO), 160.1 (CN), 155.1 (aryl-CN), 140.3 (*o*-aryl-C), 125.9 (aryl-C), 123.4 (aryl-C), 96.7 (-CH-), 27.7 [-CH(CH₃)(CH₃)'], 24.0 [-CH(CH₃)(CH₃)'], 23.6 [-CH(CH₃)(CH₃)'], 22.7 (-CH₃). IR (KBr): ν_{CO} 2053, 1988 cm⁻¹. UV-vis [CH₂Cl₂; λ_{max} /nm ($\epsilon/\text{M}^{-1}\text{cm}^{-1}$): 352 (19 600).

Synthesis of [dpp-nacnac^{CF3}]⁺Rh(CO)₂ (1b). An 8 mL ether solution containing [dpp-nacnac^{CF3}]⁺Li·Et₂O (162.0 mg, 267 μmol , 2.1 equiv) was added to a 2 mL ether suspension of [Rh(μ -Cl)(CO)₂]₂ (49.1 mg, 126 μmol , 1.0 equiv). The yellow solution was stirred for 16 h. After filtration to remove LiCl, the solvent was removed under reduced pressure. Yellow-orange crystals of the product were obtained after recrystallization of the crude product in pentane at $-35\text{ }^{\circ}\text{C}$ (yield 158.6 mg, 92%). Anal. Calcd for C₃₁H₃₅N₂O₂F₆Rh: C, 54.39; H, 5.15; N, 4.09. Found: C, 54.24; H, 5.21; N, 4.02. ¹H NMR (CDCl₃, 600 MHz): δ 7.22–7.11 (m, 6H, Ar-*H*), 6.08 (s, 1H, -*CH*-), 3.00 [sept, ³J_{HH} = 6.8 Hz, 4H, -CH(CH₃)(CH₃)'], 1.43 [d, ³J_{HH} = 6.8 Hz, 12H, -CH(CH₃)(CH₃)'], 1.26 [d, ³J_{HH} = 6.8 Hz, 12H, -CH(CH₃)(CH₃)']. ¹³C NMR (CDCl₃, 125.8 MHz): δ 180.0 (d, ¹J_{RhC} = 68 Hz, CO), 154.1 (aryl-CN), 149.2 (d, ²J_{CF} = 27 Hz, CN), 139.9 (aryl-C), 127.2 (aryl-C), 123.3 (aryl-C), 87.9 (-CH-), 28.4 [-CH(CH₃)(CH₃)'], 24.3 [-CH(CH₃)(CH₃)'], 23.3 [-CH(CH₃)(CH₃)']. ¹⁹F NMR (CDCl₃, 376.5 MHz): δ -63.5 (s, 6F, -CF₃). IR (KBr): ν_{CO} 2078, 2020 cm⁻¹. UV-vis [CH₂Cl₂; λ_{max} /nm ($\epsilon/\text{M}^{-1}\text{cm}^{-1}$): 308 (6300), 391 (12 600).

Synthesis of [dpp-nacnac^{CH3}]⁺Rh(phdi) (2a). A 50 mL methanolic solution of *N,N'*-bis(trimethylsilyl)-9,10-phenanthrenediimine (486 mg, 1.39 mmol, 1.2 equiv) and Me₃NO (174 mg, 2.32 mmol, 2.0 equiv) was stirred for 30 min. The solvent was removed under reduced pressure, and a 10 mL benzene solution of **1a** (666 mg, 1.16 mmol, 1 equiv) was added with a cannula. The yellow suspension was stirred for 24 h to afford a dark-blue suspension of the product. Dry methanol (20 mL) was added to aid product precipitation, and the product was isolated as a purple solid by filtration in air, washing with methanol, and drying under vacuum (yield 720 mg, 86%). Anal. Calcd for C₄₃H₅₁N₄Rh: C, 71.06; H, 7.07; N, 7.71. Found: C, 70.94; H, 7.23; N, 7.62. APCI-MS (toluene): *m/z* 726.1

([M]⁺). ¹H NMR (CDCl₃, 600 MHz): δ 7.98–7.90 (m, 4H, Ar-*H*), 7.82 (s, 2H, N-*H*), 7.75 (d, ²J_{HH} = 8.1 Hz, 2H, Ar-*H*), 7.71–7.67 (m, 6H, Ar-*H*), 7.22 (ddd, ⁴J_{HH} = 1.9 Hz, ³J_{HH} = 6.2 and 8.1 Hz, 2H, Ar-*H*), 4.53 (s, 1H, -*CH*-), 3.32 [sept, ³J_{HH} = 6.9 Hz, 4H, -CH(CH₃)(CH₃)'], 1.99 (s, 6H, -CH₃), 1.34 [d, ³J_{HH} = 7.0 Hz, 12H, -CH(CH₃)(CH₃)'], 0.93 [d, ³J_{HH} = 6.8 Hz, 12H, -CH(CH₃)(CH₃)']. ¹³C NMR (CDCl₃, 125.8 MHz): δ 154.6 (C-N), 153.3 (C-N), 151.6 (aryl-C-N), 145.8 (aryl-C), 130.8 (aryl-C), 129.1 (aryl-C), 129.0 (aryl-C), 126.6 (aryl-C), 125.6 (aryl-C), 124.8 (aryl-C), 122.8 (aryl-C), 118.4 (aryl-C), 97.0 (-CH-), 28.7 [-CH(CH₃)(CH₃)'], 23.8 [-CH(CH₃)(CH₃)'], 23.7 [-CH(CH₃)(CH₃)'], 23.6 (-CH₃). IR (KBr) ν 3313 (N-H) cm⁻¹. UV-vis [CH₂Cl₂; λ_{max} /nm ($\epsilon/\text{M}^{-1}\text{cm}^{-1}$): 362 (23 000), 593 (22 700), 796 (550).

Synthesis of [dpp-nacnac^{CF3}]⁺Rh(phdi) (2b). *N,N'*-Bis(trimethylsilyl)-9,10-phenanthrenediimine (80.5 mg, 0.230 mmol, 1.2 equiv) and Me₃NO (28.9 mg, 0.385 mmol, 2.0 equiv) were stirred in 10 mL of dry MeOH for 30 min. The solvent was then removed under reduced pressure, and a 3 mL benzene solution of **1b** (131.6 mg, 0.192 mmol, 1 equiv) was added with a cannula. A dark-green suspension formed and was stirred for 22 h to afford a dark-blue solution. The solution was layered with 5 mL of dry methanol to precipitate a purple solid, which was filtered in air, washed with 1 mL methanol, and dried under vacuum (yield 141.0 mg, 88%). Anal. Calcd for C₄₃H₄₅N₄F₆Rh: C, 61.87; H, 5.43; N, 6.71. Found: C, 61.53; H, 5.46; N, 6.60. ¹H NMR (CDCl₃, 600 MHz): δ 7.96–7.90 (m, 4H, Ar-*H*), 7.67 (t, ³J_{HH} = 7.5 Hz, 2H, Ar-*H*), 7.59 (d, ³J_{HH} = 7.2 Hz, 4H, Ar-*H*), 7.54 (d, ³J_{HH} = 7.8 Hz, 2H, Ar-*H*), 7.24 (d, ³J_{HH} = 9.6 Hz, 2H, Ar-*H*), 7.19 (s, 2H, N*H*), 5.56 (s, 1H, -*CH*-), 3.13 [sept, ³J_{HH} = 6.7 Hz, 4H, -CH(CH₃)(CH₃)'], 1.35 [d, ³J_{HH} = 6.8 Hz, 12H, -CH(CH₃)(CH₃)'], 0.88 [d, ³J_{HH} = 6.7 Hz, 12H, -CH(CH₃)(CH₃)']. ¹³C NMR (CDCl₃, 125.8 MHz): δ 155.7 (C-N), 149.2 (aryl-C-N), 145.4 (aryl-C), 142.4 (q, ²J_{CF} = 26 Hz, C-N), 130.3 (aryl-C), 129.6 (aryl-C), 129.3 (aryl-C), 128.7 (aryl-C), 126.5 (aryl-C), 124.7 (aryl-C), 122.4 (aryl-C), 119.2 (aryl-C), 90.3 (-CH-), 29.1 [-CH(CH₃)(CH₃)'], 24.2 [-CH(CH₃)(CH₃)'], 23.1 [-CH(CH₃)(CH₃)']. ¹⁹F NMR (CDCl₃, 376.5 MHz): δ -64.2 (s, 6F, -CF₃). IR (KBr): ν 3309 (N-H) cm⁻¹. UV-vis [CH₂Cl₂; λ_{max} /nm ($\epsilon/\text{M}^{-1}\text{cm}^{-1}$): 312 (20 000), 357 (11 100), 450 (10 700), 587 (21 100).

Synthesis of [(dpp-nacnac)Rh(phdi)][BF₄][2a][BF₄]. A 20 mL scintillation vial was charged with **2a** (104.5 mg, 144 μmol , 1 equiv) and tri-*p*-tolylammonium tetrafluoroborate (53.8 mg, 144 μmol , 1 equiv). Diethyl ether (10 mL) was added to the solids, and the blue-purple suspension was stirred for 24 h. The purple product was collected by filtration, washed with 3 \times 1.5 mL of diethyl ether, and dried under vacuum (yield 96.2 mg, 82%). IR (KBr) ν 3296 (N-H) cm⁻¹. UV-vis [CH₂Cl₂; λ_{max} /nm ($\epsilon/\text{M}^{-1}\text{cm}^{-1}$): 323 (16 334), 571 (19 700), 855 (880). EPR (CH₂Cl₂, 298 K): *g* = 2.004. EPR (CH₂Cl₂, 77 K): *g* = 2.003.

Synthesis of [K(18-crown-6)][(dpp-nacnac)Rh(phdi)] ([K(18-crown-6)][2a]). In a 20 mL scintillation vial, **2a** was dissolved in THF (105.5 mg, 145 μmol , 1 equiv) and cooled to ca. $-35\text{ }^{\circ}\text{C}$. To this deep-blue solution was added a freshly prepared K₂C₈ solid (20.1 mg, 149 μmol , 1.02 equiv). The resulting suspension was stirred for 45 min, over which time the color changed from blue to green. The solid products were then filtered off and washed with 1 mL of THF. To the filtrate was added solid 18-crown-6 (60 mg, 227 μmol , 1.6 equiv). The volume of the resulting brown solution was reduced to 4 mL in vacuo, and pentane (6 mL) was added to precipitate the product, which was filtered off, washed with pentane (3 \times 1.5 mL), and dried under vacuum (yield 143.8 mg, 96%). IR (KBr): ν 3356 (N-H) cm⁻¹. EPR (THF, 298 K): *g* = 2.09. EPR (THF, 77 K): *g* = 2.395, 1.975, and 1.941.

Crystallographic Methods. X-ray diffraction data were collected on crystals mounted on glass fibers using a Bruker CCD platform diffractometer equipped with a CCD detector. Measurements were carried out at 163 K using Mo K α (λ = 0.710 73 Å) radiation, which was wavelength-selected with a

Table 1. X-ray Diffraction Data Collection and Refinement Parameters

	[dpp-nacnac ^{CH₃]-Rh(CO)₂ (1a)}	[K(18-crown-6)] [(dpp-nacnac)Rh(phdi)] ([K(18-crown-6)] [2a])
empirical formula	C ₃₁ H ₄₁ N ₂ O ₂ Rh	C ₅₅ H ₇₅ KN ₄ O ₆ Rh•(C ₄ H ₈ O) ₃
fw	576.57	1246.51
cryst syst	monoclinic	monoclinic
space group	C2/c	P2 ₁ /c
a/Å	35.218(6)	12.5891(7)
b/Å	9.3465(16)	24.1291(13)
c/Å	20.861(4)	22.6328(12)
α/deg	90	90
β/deg	120.613(2)	105.2230(10)
γ/deg	90	90
V/Å ³	5909.8(17)	6633.8(6)
Z	8	4
reflins collected	31 653	76 342
indep reflins	7286	15 768
R1 [I > 2σ(I)] ^a	0.0209	0.0376
wR2 (all data) ^a	0.0554	0.0874
GOF ^a	1.052	0.997

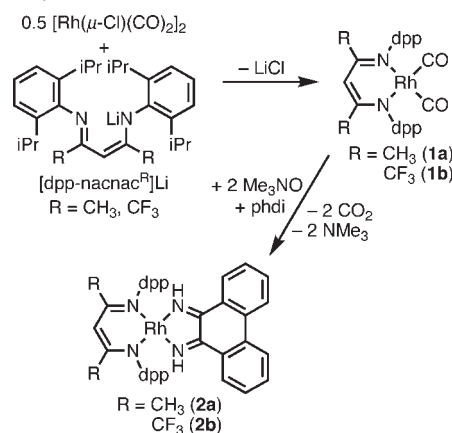
$${}^a R1 = \frac{\sum ||F_o| - |F_c||}{\sum |F_o|}; wR2 = \frac{[\sum [w(F_o^2 - F_c^2)^2]]^{1/2}}{[\sum w(F_o^2)]^{1/2}};$$

$$GOF = \frac{[\sum w(|F_o| - |F_c|)^2 / (n - m)]^{1/2}}{}$$

single-crystal graphite monochromator. The *SMART* program package was used to determine unit-cell parameters and to collect data.²² The raw frame data were processed using *SAINTE*²³ and *SADABS*²⁴ to yield the reflection data files. Subsequent calculations were carried out using the *SHELXTL*²⁵ program suite. Structures were solved by direct methods and refined on F^2 by full-matrix least-squares techniques. Analytical scattering factors for neutral atoms were used throughout the analyses.²⁶ Hydrogen atoms were included using a riding model. ORTEP diagrams were generated using *ORTEP-3* for Windows.²⁷ Diffraction data are shown in Table 1.

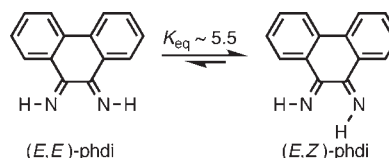
Results

Synthesis and Characterization of Rh^Iphdi Complexes. phdi was synthesized in quantitative yield by stirring *N,N'*-bis(trimethylsilyl)-9,10-phenanthrenediimine in dry methanol.¹⁶ Removal of the methanol in vacuo resulted in a quantitative yield of phdi, which is pure by ¹H NMR spectroscopy. Incorporation of deuterium into the imine group was readily achieved using CH₃OD for deprotection. The free ligand exists as a mixture of *E,Z* and *E,E* isomers in a 5.5:1 ratio (eq 1), as determined by ¹H NMR spectroscopy at 298 K in deuterated benzene ($\Delta G^\circ = 1.0 \text{ kcal mol}^{-1}$).¹⁷ Deuterium substitution to make phdi-*d*₂ favors the *E,Z* isomer further (6.6:1), consistent with stronger hydrogen bonding in the deuterated compound.²⁸ The symmetric *E,E* isomer shows five equal-intensity ¹H NMR resonances in the aromatic region, whereas the asymmetric *E,Z* isomer shows 10

Scheme 1. Synthesis of **2a** and **2b****Table 2.** Selected Bond Lengths (Å) for **1a** and [K(18-crown-6)]**[2a]**

	1a	[K(18-crown-6)] [2a]
Rh(1)–N(1)	2.0491(11)	2.0097(16)
Rh(1)–N(2)	2.0514(11)	2.0111(16)
Rh(1)–N(3)		1.9881(17)
Rh(1)–N(4)		1.9832(17)
N(1)–C(1)	1.3308(16)	1.332(3)
N(2)–C(3)	1.3316(17)	1.331(2)
C(1)–C(2)	1.3994(16)	1.394(3)
C(2)–C(3)	1.3965(17)	1.401(3)
N(3)–C(30)		1.350(2)
N(4)–C(43)		1.349(3)
C(30)–C(43)		1.409(3)

equal-intensity ¹H NMR resonances. The N–H protons of the *E,E* isomer resonate at 10.2 ppm, but hydrogen bonding in the *E,Z* isomer splits the N–H proton resonances, which appear at 10.5 and 12.4 ppm, respectively.



Metalation of phdi with rhodium(I) was achieved by oxidative decarbonylation of **1a** and **1b** (Scheme 1). Complex **1a** was prepared from [Rh(μ -Cl)(CO)₂]₂ and [dpp-nacnac]Li·Et₂O in 78% yield according to procedures developed for other Rh-nacnac derivatives.^{12a} Similarly, the derivative with the fluorinated nacnac ligand, **1b**, was synthesized in 92% yield by stirring [Rh(μ -Cl)(CO)₂]₂ with [dpp-nacnac^{CF₃}]₂Li·Et₂O overnight at room temperature. The geometry of the Rh-nacnac unit in **1a**, determined by single-crystal X-ray diffraction (see the Supporting Information) is roughly square-planar and analogous to other previously reported Rh^Inacnac derivatives.^{12a,b,29} Selected metrical data for **1a** are shown in Table 2. IR spectra of **1a** and **1b** revealed two C≡O stretching frequencies, observed at 2053 and 1988 cm⁻¹ for **1a** and at 2078 and 2020 cm⁻¹ for **1b** ($\Delta\nu = 25$ and 32 cm⁻¹, respectively). The observed blue shift in the

(22) *SMART Software Users Guide*, version 5.1; Bruker Analytical X-ray Systems, Inc.: Madison, WI, 1999.

(23) *SAINTE Software Users Guide*, version 6.0; Bruker Analytical X-ray Systems, Inc.: Madison, WI, 1999.

(24) Sheldrick, G. M. *SADABS*, version 2.10; Bruker Analytical X-ray Systems, Inc.: Madison, WI, 2002.

(25) Sheldrick, G. M. *SHELXTL*, version 6.12; Bruker Analytical X-ray Systems, Inc.: Madison, WI, 2001.

(26) *International Tables for X-Ray Crystallography*; Kluwer Academic Publishers: Dordrecht, The Netherlands, 1992; Vol. C.

(27) Farrugia, L. J. *J. Appl. Crystallogr.* **1997**, *30*, 565.

(28) (a) Pal, H.; Nagasawa, Y.; Tominaga, K.; Kumazaki, S.; Yoshihara, K. *J. Chem. Phys.* **1995**, *102*, 7758–7760. (b) Rao, C. N. R. *J. Chem. Soc., Faraday Trans. 1* **1975**, *71*, 980–983. (c) Némethy, G.; Scheraga, H. A. *J. Chem. Phys.* **1964**, *41*, 680–689.

(29) (a) Geier, S. J.; Stephan, D. W. *Chem. Commun.* **2008**, 99–101. (c) Willems, S. T. H.; Budzelaar, P. H. M.; Moonen, N. N. P.; de Gelder, R.; Smits, J. M. M.; Gal, A. W. *Chem.—Eur. J.* **2002**, *8*, 1310–1320. (d) Budzelaar, P. H. M.; Moonen, N. N. P.; de Gelder, R.; Smits, J. M. M.; Gal, A. W. *Eur. J. Inorg. Chem.* **2000**, 753–769.

C≡O stretching frequencies for **1a** and **1b** indicates that the electronic properties of the nacnac ligands have a pronounced impact on the electron density at the metal center, and the installation of CF₃ groups into the nacnac backbone affords a more electron-deficient rhodium center that cannot π -backbond as strongly to the carbonyl ligands. For comparison, the two C≡O stretching frequencies for the analogous iridium complexes, [dpp-nacnac^{CH₃}Ir(CO)₂] and [dpp-nacnac^{CF₃}Ir(CO)₂], only blue shift by 20 and 16 cm⁻¹, respectively,³⁰ indicating a much smaller interaction of the nacnac ligand with the metal valence orbitals.

Compounds **1a** and **1b** are robust in the presence of phdi; however, Me₃NO can be added to promote reaction through the oxidative removal of carbonyl ligands (Scheme 1). The addition of 2 equiv of Me₃NO to a benzene solution of **1a** and phdi resulted in the release of CO₂ and formation of **2a** as a microcrystalline purple solid in 73% isolated yield. Complex **2a** can also be prepared directly using the crude phdi product obtained upon removal of methanol from deprotection of *N,N'*-bis(trimethylsilyl)-9,10-phenanthrenediimine. The yield of **2a** prepared in this manner is 86% based on **1a**. The reaction of **1b** with phdi and 2 equiv of Me₃NO proceeds similarly to afford **2b** as a purple solid in 88% yield.

Complexes **2a** and **2b** are proposed to be square-planar rhodium complexes. The formulation of both complexes was confirmed by elemental analysis and atmospheric-pressure chemical ionization mass spectrometry (APCI-MS), which showed [M]⁺ peaks with the appropriate isotopic distribution at *m/z* 726.1 for **2a** and *m/z* 834.2 for **2b**. The ¹H NMR spectra of **2a** and **2b** are consistent with C_{2v}-symmetric, square-planar complexes and show chemical shifts similar to those of the dicarbonyl complexes **1a** and **1b**. Spectra of **2a** and **2b** show four equivalent isopropyl groups for the dpp-nacnac ligands with single methine resonances at 3.32 and 3.13 ppm, respectively. The diastereotopic methyl resonances are observed at 0.93 and 1.34 ppm for **2a** and at 0.88 and 1.35 ppm for **2b**. In both cases, the phdi ligand is symmetric with four aromatic resonances. The most significant differences in the ¹H NMR spectra of the two complexes are in the chemical shifts of the phdi N–H resonances and the vinylic nacnac C–H resonance. Whereas the vinylic C–H resonance of **2b** (5.56 ppm) shifts downfield relative to the same resonance in **2a** (4.53 ppm), the phdi N–H resonance of **2b** (7.19 ppm) is shifted upfield compared to **2a** (7.82 ppm). While it would be desirable to track the synthesis and reactivity of **2a** and **2b** by monitoring the C=N stretches of the phdi ligand, these stretches are less prominent than the CO ligands of **1a** and **1b** and are red-shifted into the fingerprint region of the complexes, making definitive assignments difficult. The N–H stretches are readily visible in the IR spectrum at 3313 cm⁻¹ for **2a** and at 3309 cm⁻¹ for **2b**.

The UV–vis spectra of **2a** and **2b**, shown in Figure 1, display several intense transitions throughout the visible region of the spectrum. In the case of **2a**, two strong charge-transfer transitions were observed at 362 nm (23 000 M⁻¹ cm⁻¹) and 593 nm (22 700 M⁻¹ cm⁻¹) along with two or more shoulders in the 400–450 nm range and a weak transition at 796 nm (546 M⁻¹ cm⁻¹). The UV–vis spectrum of **2b** is similar,

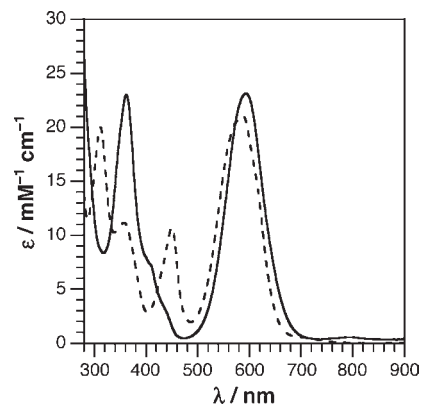


Figure 1. UV–vis spectra of **2a** (solid line) and **2b** (dashed line) at 298 K in CH₂Cl₂.

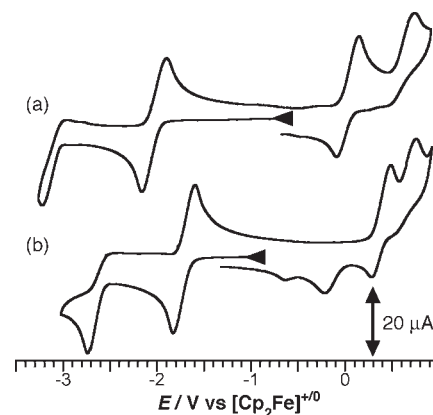


Figure 2. Cyclic voltammograms of (a) **2a** and (b) **2b** measured at 200 mV s⁻¹. All measurements were made in a THF solution with 1.0 mM analyte and 0.10 M TBAPF₆ under an inert atmosphere. Potentials were referenced to [Cp₂Fe]^{0/+}.

showing transitions at 312 nm (20 000 M⁻¹ cm⁻¹) and 587 nm (21 100 M⁻¹ cm⁻¹); furthermore, two additional strong transitions are observed at 357 nm (11 100 M⁻¹ cm⁻¹) and 450 nm (10 700 M⁻¹ cm⁻¹). That the high-energy band shifts from 362 nm in **2a** to 312 nm in **2b** suggests that this transition originates on the metal or the nacnac ligand, with the CF₃ groups of [dpp-nacnac^{CF₃}] causing the 50 nm blue shift in **2b**. The small blue shift of the low-energy band on going from **2a** to **2b** suggests a metal-to-ligand charge-transfer assignment involving only the rhodium center and the phdi ligand.

Electrochemical Studies of 2a and 2b. Cyclic voltammetry studies were conducted on solution samples of **2a** and **2b** to probe their outer-sphere redox properties. The juxtaposition of a low-valent rhodium metal center and a reducible phdi ligand in complexes **2a** and **2b** suggests that both oxidative and reductive processes might be accessible. The cyclic voltammogram of **2a** in THF is shown in Figure 2a. A reversible one-electron reduction was observed at –2.03 V along with a reversible one-electron oxidation at 0.06 V (all potentials vs [Cp₂Fe]^{+/0}).³¹ Furthermore, an irreversible oxidative process and a partially reversible reductive process can be observed near the edges of the solvent window at +0.79 and –3.08 V, respectively. The cyclic voltammogram of **2b**, shown in Figure 2b, is similar, showing a reversible

(30) Bernskoetter, W. H.; Lobkovsky, E.; Chirik, P. J. *Organometallics* 2005, 24, 6250–6259.

(31) All potentials referenced to the [Cp₂Fe]^{+/0} redox couple using Cp*₂Fe (E_{1/2} = –0.49 V) as an internal standard.

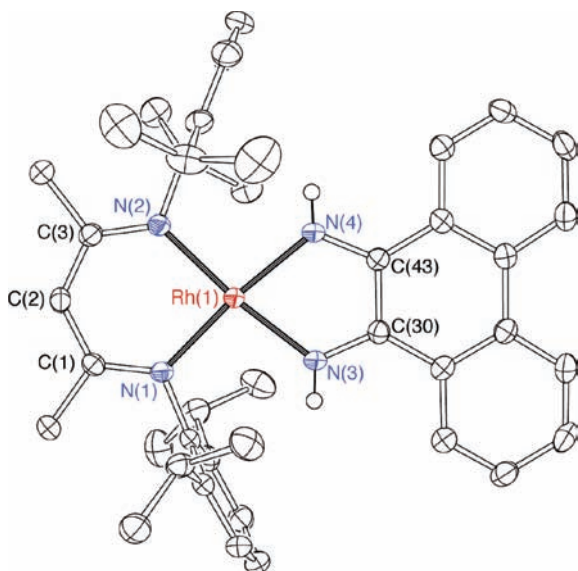


Figure 3. ORTEP plot of the rhodium anion $[2a]^-$. Ellipsoids are shown at 50% probability. The $[K(18\text{-crown-6})]$ cation, a THF molecule, and all carbon-bound hydrogen atoms have been omitted for clarity.

one-electron reduction at -1.79 V. The first one-electron oxidation, at $+0.37$ V, is only partially reversible, as is the second reduction at -2.69 V. The second oxidative process ($+0.75$ V) is irreversible, as with **2a**. Finally, the cyclic voltammogram of **2b** shows daughter reductions at -0.27 and -0.6 V spawned from the second irreversible oxidation at $+0.75$ V.³² The reductive processes observed for **2a** and **2b** are consistent with the cyclic voltammetry results obtained for the free phdi ligand, which showed a partially reversible reduction at -1.94 V and an irreversible reduction at -2.66 V. As expected, the incorporation of CF_3 -substituted nacnac ligand into the rhodium coordination sphere makes the complex both easier to reduce and harder to oxidize, consistent with a more electron-deficient metal center.

Outer-Sphere Oxidation and Reduction of 2a. The reversibility of the first oxidation and reduction processes in the cyclic voltammogram of **2a** suggested that the products of these process species might be isolable. The chemical reduction of **2a** requires a powerful reductant and was achieved by reaction with 1 equiv of KC_8 . The addition of 18-crown-6 to a THF solution of the reduction product afforded green crystals of $[K(18\text{-crown-6})][2a]$ in 96% yield. Single crystals of $[K(18\text{-crown-6})][2a]$ were grown from a saturated THF solution and analyzed by X-ray diffraction. The structure of the rhodium complex anion is depicted as an ORTEP plot in Figure 3. Table 2 lists selected bond distances and angles for the rhodium complex anion. The Rh–N bond distances to the nacnac^{CH₃} ligand in $\{[dpp\text{-nacnac}^{CH_3}]Rh(\text{phdi})\}^- ([2a]^-)$ are significantly shorter (2.01 Å) than the analogous Rh–N bond distances to the nacnac^{CH₃} ligand in the neutral dicarbonyl complex **1a** (2.05 Å). Other metrical parameters for the nacnac^{CH₃} ligand of $[2a]^-$ match up well with those in **1a**. Within the phdi ligand, the C–N distances are long (1.35 Å), consistent with the reduction of the diimine functionality of the ligand. Furthermore, the C(30)–C(43) distance of 1.41 Å is consistent with an aromatic C–C bond

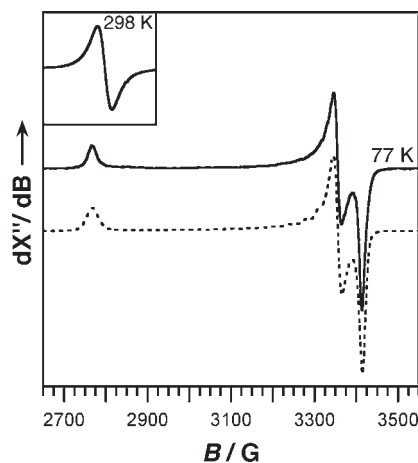


Figure 4. X-band EPR spectrum of $[2a]^-$ in THF at 77 and 298 K (inset). The best fit for the 77 K spectrum (dashed line) was obtained with $g_x = 2.39$, $g_y = 1.97$, and $g_z = 1.94$.

suggestive of a doubly reduced phdi ligand in $[2a]^-$. Similar C–N and C–C bond distances in redox-active diimine ligands have been taken as evidence for the reduction of the ligand to the semiquinonate or even the catecholate oxidation state.^{15,33,34} For comparison, rhodium complexes with phdi ligands typically show a C=N bond distance of 1.29 Å and a C–C bond distance of 1.49 Å.^{13c,35}

Complex $[2a]^-$ was characterized by solution EPR and solid-state IR spectroscopy. The IR spectrum showed the N–H stretch at 3356 cm^{-1} ; however, no clearly assignable C=N stretch was observed. Figure 4 shows the solution X-band EPR spectrum at 77 and 298 K (inset), obtained for crystals of $[K(18\text{-crown-6})][2a]$ dissolved in THF. At 298 K, the EPR spectrum of $[2a]^-$ shows a broad signal at $g = 2.09$. Upon cooling to 77 K, the signal becomes rhombic with features at $g = 2.39$, 1.97, and 1.94. For comparison, related square-planar rhodium(I) semiquinonate complexes, $[sq]^-Rh^I(CO)_2$ ($[sq]^- = 3,5\text{-di-}tert\text{-butyl-1,2\text{-semiquinonate}}$ and substituted derivatives), have been reported to show isotropic EPR spectra ($g = 2.002$) with well-defined hyperfine coupling to the semiquinonate ligand substituents, indicative of the unpaired electron residing on the redox-active ligand.³⁶ Similarly, rhodium(0) complexes typically show isotropic or axial EPR spectra with g values close to 2.0 at both room and low temperature.^{37–40} In contrast, rhodium(II) complexes typically show rhombic EPR spectra at low

(33) (a) Jüstel, T.; Bendix, J.; Metzler-Nolte, N.; Weyhermüller, T.; Nuber, B.; Wieghardt, K. *Inorg. Chem.* **1998**, *37*, 35–43. (b) Chopek, K.; Bothe, E.; Neese, F.; Weyhermüller, T.; Wieghardt, K. *Inorg. Chem.* **2006**, *45*, 6298–6307.

(34) Bhattacharya, S.; Gupta, P.; Basuli, F.; Pierpont, C. G. *Inorg. Chem.* **2002**, *41*, 5810–5816.

(35) (a) Kisko, J. L.; Barton, J. K. *Inorg. Chem.* **2000**, *39*, 4942–4949. (b) Krotz, A. H.; Barton, J. K. *Inorg. Chem.* **1994**, *33*, 1940–1947.

(36) (a) Bubnov, M. P.; Nevodchikov, V. I.; Fukin, G. K.; Cherkasov, V. K.; Abakumov, G. A. *Inorg. Chem. Commun.* **2007**, *10*, 989–992. (b) Abakumov, G. A.; Nevodchikov, V. I. *Dokl. Acad. Nauk* **1982**, *266*, 1407–1410. (37) Căldăraru, H.; Dearmond, M. K.; Hanck, K. W.; Sahini, V. E. *J. Am. Chem. Soc.* **1976**, *98*, 4455–4457.

(38) (a) Kunin, A. J.; Nanni, E. J.; Eisenberg, R. *Inorg. Chem.* **1985**, *24*, 1852–1856. (b) Mueller, K. T.; Kunin, A. J.; Greiner, S.; Henderson, T.; Kreilick, R. W.; Eisenberg, R. *J. Am. Chem. Soc.* **1987**, *109*, 6313–6318.

(39) Longato, B.; Coppo, R.; Pilloni, G.; Corvaja, C.; Toffoletti, A.; Bandoli, G. *J. Organomet. Chem.* **2001**, *637*, 710–718.

(40) (a) Deblon, S.; Liesum, L.; Harmer, J.; Schönberg, H.; Schweiger, A.; Grützmacher, H. *Chem.—Eur. J.* **2002**, *8*, 601–611. (b) de Bruin, B.; Russcher, J. C.; Grützmacher, H. *J. Organomet. Chem.* **2007**, *692*, 3167–3173.

(32) Daughter peaks are also observed on the second cyclic scan of **2a** at -0.45 , -0.85 , and -1.28 V.

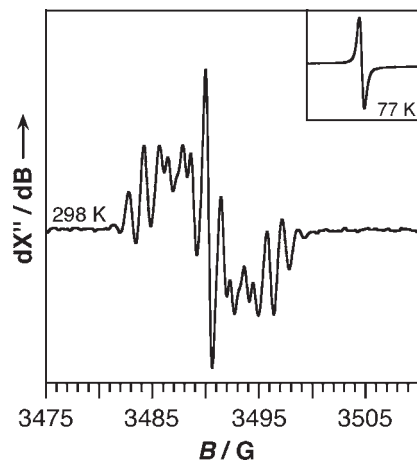


Figure 5. X-band EPR spectrum of $[2a]^+$ in CH_2Cl_2 at 298 and 77 K (inset).

temperatures.⁴¹ The EPR parameters for $[2a]^-$ are similar to those of the recently reported planar rhodium dianion $[Rh\{bdt\}_2]^{2-}$ ($\{bdt\}^{2-} = 3,6\text{-bis}(\text{trimethylsilyl})\text{benzene-1,2-dithiolate}$), which was assigned a rhodium(II) oxidation state based on a rhombic EPR spectrum at 25 K with $g = 2.50, 2.00,$ and 1.97 .⁴²

One-electron oxidation of **2a** was possible using tri-*p*-tolylammonium as an oxidant. While the electrochemical data shown in Figure 2 suggest that silver salts would be competent oxidants for **2a**, reactions using these reagents did not lead to clean oxidation of the rhodium complex. On the other hand, $[N(p\text{-tolyl})_3][BF_4]$ reacted cleanly with **2a** to provide the oxidized product as a purple paramagnetic solid, $\{[dpp\text{-nacnac}^{CH_3}Rh(\text{phdi})]\{BF_4\}\} ([2a][BF_4])$ in 82% yield. The new species was characterized by solid-state IR spectroscopy, UV-vis electronic spectroscopy, and solution-phase EPR spectroscopy. The N-H stretch is shifted to 3296 cm^{-1} in the IR spectrum. The UV-vis spectrum of $\{[dpp\text{-nacnac}^{CH_3}]Rh(\text{phdi})\}^+ ([2a]^+)$ is similar to that of **2a**, showing two intense transitions at 327 nm ($16\,000\text{ M}^{-1}\text{ cm}^{-1}$) and 571 nm ($19\,700\text{ M}^{-1}\text{ cm}^{-1}$). The X-band EPR spectrum of $[2a]^+$ at 298 K, shown in Figure 5, displayed an isotropic 15-line signal centered at $g = 2.004$. Upon cooling to 77 K, this complex signal simplified to a single, sharp, isotropic signal centered at $g = 2.003$. The EPR data for $[2a]^+$ is again indicative of an $S = 1/2$ complex; however, the g value and isotropic nature of the signal are not consistent with localization of the unpaired electron on the metal center to afford a rhodium(II) complex. Instead, the EPR signal, with sharp hyperfine couplings that disappear at low temperature, is consistent with delocalization of the unpaired electron onto the organic ligand framework.

Discussion

Complexes **2a** and **2b** present an interesting opportunity to evaluate the electronic structure and reactivity of a

nucleophilic metal center coordinated to an electrophilic or reducible ligand. Typically, square-planar d^8 transition-metal complexes are nucleophilic because of the nonbonding electron pair held within the metal d_{z^2} orbital. On the other hand, the coordinated phdi ligand, an α -diimine analogous to phenanthrenequinone, has a low-energy π^* orbital capable of accepting two electrons. The juxtaposition of these two motifs may offer the ability to design new catalysts that take advantage of both the nucleophilic properties and the ability to act as two-electron oxidants. In order to develop our understanding of how metal and ligand fragments can work together, we examined the structural, spectroscopic, and electronic properties of **2a** and **2b**.

Comparisons between **2a** and **2b** were used to determine to what extent the nacnac ligand impacts the electronic structure of the Rh-phdi unit. According to the CO stretching frequencies in **1a** and **1b**, substitution of CF_3 groups into the nacnac backbone has a strong impact on the ability of the rhodium center to participate in π -backbonding with the CO ligands. The nacnac ligands should have an analogous impact in **2a** and **2b** and modulate the electronic interaction between the rhodium centers and the redox-active phdi ligand. While the C=N stretching frequencies of **2a** and **2b** cannot be used to probe the difference between **2a** and **2b**, the N-H stretching frequency decreases upon substitution of the fluorinated ligand, suggesting that ν_{N-H} is a strong indicator of Rh \rightarrow phdi electron donation. Cyclic voltammetry data support the contention that **2b** is more electron-deficient than **2a**, with one-electron-oxidation and -reduction potentials shifting by +310 and +240 mV, respectively, for **2b** relative to **2a**. These data suggest that subtle changes to an auxiliary ligand coordinated to the Rh-phdi fragment can have dramatic effects on the electronic properties of the overall complex.

The key aspect of these studies was to probe the nature of the Rh-phdi interaction. The "formal" oxidation state assignment for **2a** and **2b** would be that of a rhodium(I) coordinated to a neutral phdi ligand (**A** in Chart 2),⁴³ however, this formal oxidation state assignment does not necessarily correspond to the "experimental" oxidation state of the complex.⁴⁴ An alternative, electronic isomer⁴⁵⁻⁴⁷ for **2a** and **2b** would be an antiferromagnetically coupled, biradical state with a rhodium-(II) coordinated to a $[phdisq]^-$ ligand (**B** in Chart 2). In the absence of high-resolution structural data for **2a** or **2b**, distinguishing between **A** and **B** is difficult,⁴⁸ and our spectroscopic

(43) (a) Hegedus, L. S. In *Transition Metals in the Synthesis of Complex Organic Molecules*; University Science Books: Mill Valley, CA, 1994; p 3. (b) Shriver, D.; Atkins, P. In *Inorganic Chemistry*, 3rd ed.; W. H. Freeman: New York, 1999; p 69.

(44) (a) Jørgensen, C. K. In *Oxidation Numbers and Oxidation States*; Springer: Heidelberg, Germany, 1969. (b) Chaudhuri, P.; Verani, C. N.; Bill, E.; Bothe, E.; Weyhermüller, T.; Wieghardt, K. *J. Am. Chem. Soc.* **2001**, *123*, 2213–2223.

(45) We use the term "electronic isomer" to indicate a specific distribution of electrons for the complex as represented by a given Lewis structure. The terms "valence tautomer" (see ref 46) and "electromer" (see ref 47) also have been used in the literature to indicate species with the same arrangement of nuclei but different distributions of electrons.

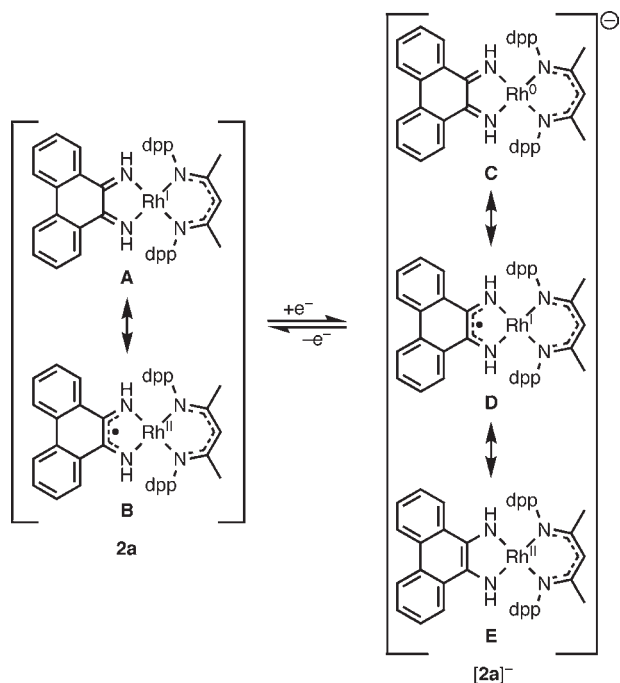
(46) Pierpont, C. G. *Coord. Chem. Rev.* **2001**, *216–217*, 99–125.

(47) Bally, T. *Nat. Chem.* **2010**, *2*, 165–166.

(48) Attempts to resolve the issue of the two electronic isomers through high-level density functional theory calculations have led to ambiguous results. Both closed-shell $Rh^I\text{phdi}$ and biradical $Rh^{II}\text{phdisq}^-$ structures have been located; however, the energy differences are within the error of the calculation. A further complication arises in that the electronic structures of each electronic isomer show a strong dependence on the functional employed for the calculation.

(41) (a) Wayland, B. B.; Sherry, A. E.; Bunn, A. G. *J. Am. Chem. Soc.* **1993**, *115*, 7675–7684. (b) Dixon, F. M.; Farrell, J. R.; Doan, P. E.; Williamson, A.; Weinberger, D. A.; Mirkin, C. A.; Stern, C.; Incarvito, C. D.; Liable-Sands, L. M.; Zakharov, L. N.; Rheingold, A. L. *Organometallics* **2002**, *21*, 3091–3093. (c) Gerisch, M.; Krumper, J. R.; Bergman, R. G.; Tilley, T. D. *Organometallics* **2003**, *22*, 47–58. (d) Hettterscheid, D. G. H.; Klop, M.; Kicken, R. J. N. A. M.; Smits, J. M. M.; Reijerse, E. J.; de Bruin, B. *Chem.—Eur. J.* **2007**, *13*, 3386–3405.

(42) Benedito, F. L.; Petrenko, T.; Bill, E.; Weyhermüller, T.; Wieghardt, K. *Inorg. Chem.* **2009**, *48*, 10913–10925.

Chart 2. Possible Electronic Isomers for **2a** and $[2a]^-$ 

data provide scant evidence for favoring biradical **B** over the formal electronic isomer **A**. Neither complex **2a** nor **2b** shows evidence for paramagnetism that would arise from breaking of the antiferromagnetic interaction in biradical isomer **B**. Similarly, the NMR spectra of **2a** and **2b** show no evidence for paramagnetically shifted resonances that might occur for a $[\text{nacnac}]^-$ ligand coordinated to a rhodium(II) center; furthermore, the $[\text{nacnac}]^-$ features in the NMR spectra of **2a** and **2b** are very similar to those in the spectra of **1a** and **1b**, where a biradical representation like **B** is not plausible. The resonances for the redox-active ligand in **2a** and **2b** also are consistent with those for the free phdi ligand. While the lowest-energy transition in the UV-vis spectra of **2a** and **2b** shows barely any change between **2a** and **2b**, opening the possibility of an intraligand charge-transfer transition within an open-shell $[\text{phdisq}]^-$ ligand, the energy of this transition is in line with other rhodium(I) α -diimine complexes,⁴⁹ suggesting a better assignment as metal-to-diimine-ligand charge transfer.

Characterization of the anion $[2a]^-$ is straightforward because of the characteristic $S = 1/2$ EPR signature of the reduced complex and proves the accessibility of a rhodium(II) oxidation state. The extra electron in the anion $[2a]^-$ should be contained within a molecular orbital localized on the phdi ligand or on the rhodium metal center. The Lewis structures for three potential electronic isomers of $[2a]^-$ are shown in Chart 2. If **2a** is viewed as $\text{Rh}^{\text{I}}\text{phdi}$ isomer **A**, reduction at the metal center would leave the phdi ligand in the diimine oxidation state while reducing the metal center to a d^9 rhodium(0) isomer, **C**. The other possibility for the reduction of **A** is to place the electron into the π system of the phdi ligand, reducing it from a diimine to a diiminosemiquinonate ligand and leaving the metal as a d^8 rhodium(I) isomer, **D**. The same electronic isomer of $[2a]^-$, **D**, would be generated by the metal-based reduction of $\text{Rh}^{\text{II}}[\text{phdisq}]^-$,

isomer **B** of **2a**. The ligand-based reduction of **B** would generate isomer **E**, comprising a rhodium(II) metal center and a fully reduced $[\text{phda}]^{2-}$ ligand.

Both EPR spectroscopic and X-ray structural data support **E** as the best description for $[2a]^-$. Most proposed rhodium(0) complexes in the literature are highly delocalized, with the unpaired electron spread out over the metal and ligands.⁴⁰ Both electronic isomers **C** and **D** would be expected to give rise to an isotropic or axial EPR spectrum at high and low temperatures, with g value(s) very close to 2.0, as has been observed for other delocalized rhodium(0) complexes and square-planar metal complexes with semiquinonate ligands.^{37–40} Conversely, anion $[2a]^-$ displays an isotropic EPR spectrum at room temperature that becomes rhombic upon cooling to 77 K. The observed g values and degree of rhombicity are consistent with EPR spectra of d^7 rhodium(II) complexes reported in the literature.^{41,42} It is surprising that the reduction of **2a** affords an anion with clear rhodium(II) character, but two factors could work to stabilize electronic isomer **E** relative to **C/D**. First, the $[\text{phda}]^{2-}$ ligand is a closed-shell phenanthrene ring system, which would benefit from full aromatic stabilization energy. Second, **E** places two electrons in a π -type ligand orbital rather than the d_z^2 orbital that is localized on the rhodium center. Placing two electrons in a π -type orbital should result in less electron-pair repulsion because the electrons are delocalized over a larger volume.

Conclusion

Definitive assignments of experimental oxidation states for **2a** and **2b** are problematic. Given the results of related work on square-planar d^8 complexes of palladium and platinum,^{50,51} it is tempting to assign a closed-shell, $\text{Rh}^{\text{I}}\text{phdi}$ ground-state electron configuration for **2a** and **2b**. On the other hand, square-planar rhodium complexes with redox-active dithiolene ligands seem to show a proclivity for the d^7 rhodium(II) oxidation state.⁴² While there is no definitive structural or spectroscopic evidence for assigning the $\text{Rh}^{\text{II}}[\text{phdisq}]^-$ electronic isomer (**B** of Chart 2) as the ground state for **2a** and **2b**, the electrochemically reversible reduction of **2a** and characterization of the product, $[2a]^-$, as a $\text{Rh}^{\text{II}}[\text{phda}]$ complex suggest that **2a** has at least some biradical character in the ground state. Hence, the individual $\text{Rh}^{\text{I}}\text{phdi}$ (**A**) and $\text{Rh}^{\text{II}}[\text{phdisq}]^-$ (**B**) electronic isomers of **2a** are too simple and a limitation of Lewis structures in representing the electronic structure of complex molecules. Instead, the ground state of **2a** likely has character of both electronic isomers **A** and **B** and should be represented as a multiconfiguration ground state.⁵¹ Within the framework of Lewis structures, this multiconfigurational character can be represented with resonance, as is often done to overcome the limitations of Lewis structures in explaining the reactivity of organic molecules.

Undoubtedly, coordination of the phdi ligand to a square-planar rhodium(I) generates a molecular platform with interesting electronic properties. As expected, the proximity of metal- and phdi-based valence orbitals leads to electronic structures that include a wealth of charge-transfer character and that are capable of reversible outer-sphere oxidation and

(49) (a) Shinozaki, K.; Takahashi, N. *Inorg. Chem.* **1996**, *35*, 3917–3924. (b) Fordyce, W. A.; Crosby, G. A. *Inorg. Chem.* **1982**, *21*, 1023–1026. (c) Kaim, W.; Reinhardt, R.; Sieger, M. *Inorg. Chem.* **1994**, *33*, 4453–4459. (d) Ladwig, M.; Kaim, W. *J. Organomet. Chem.* **1991**, *419*, 233–243.

(50) (a) Ghosh, P.; Begum, A.; Herebian, D.; Bothe, E.; Hildenbrand, K.; Weyhermüller, T.; Wieghardt, K. *Angew. Chem., Int. Ed.* **2003**, *42*, 563–567. (b) Herebian, D.; Bothe, E.; Neese, F.; Weyhermüller, T.; Wieghardt, K. *J. Am. Chem. Soc.* **2003**, *125*, 9116–9128.

(51) Ray, K.; Weyhermüller, T.; Neese, F.; Wieghardt, K. *Inorg. Chem.* **2005**, *44*, 5345–5360.

reduction processes. Regardless of the electronic configuration assignment that is made for the members of the $[2a]^+$, **2a**, and $[2a]^-$ redox series, the stability of the [nacnac]Rh(phdi) core through multiple one-electron processes motivates further studies into the reactivity of the Rh-phdi platform.

Acknowledgment. This work was supported by the UCI School of Physical Sciences Center for Solar Energy. A.F.H.

is an Alfred P. Sloan Foundation Fellow and a Camille Dreyfus Teacher–Scholar. The authors thank Heraeus for donation of the rhodium starting material.

Supporting Information Available: X-ray crystal structure, listing of bond lengths, and cyclic voltammetry data for **1a**. This material is available free of charge via the Internet at <http://pubs.acs.org>.